Journal of
Computational and Theoretical Nanoscience
Vol. 6, 1–10, 2009

Uncertainty Quantification of the Subsurface Failure of Composites with Nanoscale Constituents

D. Arbelaez* and T. I. Zohdi

Department of Mechanical Engineering, University of California, Berkeley, CA, 94720-1740, USA

This paper investigates the uncertainty in the subsurface damage of composite materials containing randomly dispersed nanoscale particles. In the design of such materials, there is an inherent uncertainty in their effective response, due to the uncertainty in the geometry and distribution of matrix-embedded small-scale particles. In this work, a model is developed to estimate the effect of second phase particles on the amount of material that is damaged directly beneath the subsurface of a nanoheterogeneous material, due to surface loading. The approach is to construct a mesoscale stress distribution within a solid using effective material properties. Stress concentration functions are then developed in order to explicitly determine the extent of failed binding matrix material, as a function of the intensity of the loading. Afterwards, the sensitivity of this model to the uncertainty in the effective properties of the composite material is examined. In this model, the amount of subsurface damage depends on the effective Poisson ratio and a stress concentration function. It is found that the amount of subsurface damage is highly sensitive to variations in this stress concentration function which is strongly dependent on the particulate volume fraction and the ratio of the shear moduli. Therefore, the uncertainty in the amount of subsurface volume damaged is strongly dependent on the volume fraction of the particulate phase and the ratio of the shear moduli of the two phases and weakly dependent on the ratio of the bulk moduli.

Keywords: Subsurface, Nanoscale Particles, Nanocomposites.

RESEARCH ARTICLE

1. INTRODUCTION

Recently, the use of nanoparticles to reinforce a matrix material has received considerable attention due to the unique properties that these materials exhibit. Several researchers have shown that nanoparticle reinforced metals may exhibit greater strength when compared to composites with micro sized particles. For example, Hassan and Gupta,[1] Hwang et al.,[2] Lu et al.,[3] and Shao et al.[4] However, at these size scales it is difficult to ascertain what the effective (homogenized) properties of the material will be due to the uncertainty in the morphology and distribution of these particles within the composite material. For example, even at moderate volume fractions the particles are known to agglomerate and form clusters inside of the matrix material.[5] In this work, the uncertainty in subsurface damage, due to a surface force, of composite materials containing randomly dispersed particles to the uncertainty in the microstructural morphology and therefore the effective material properties is investigated.

Several researchers have studied the effect of particle size on the yield strength of metal matrix nanocomposites. In general the yield strength can be described as $\sigma_c = \sigma_m(1 + f_1)$, where the factor f_1 primarily depends on volume fraction and σ_m is the enhanced strength of the reinforced matrix. The parameter σ_m depends on both the differential loading between the binding phase and inclusions, as well as the particle size dependent strengthening in the matrix material, due to enhanced dislocation density.[6] In this paper, a micromechanics approach is used to determine how the load is shared between the matrix material and the particulate inclusions in a mean sense. For this purpose, a stress concentration tensor, $\bar{\bar{C}}$, is derived such that $\langle \boldsymbol{\sigma} \rangle_{\Omega_1} = \bar{\bar{C}} : \langle \boldsymbol{\sigma} \rangle_{\Omega}$, where $\langle \boldsymbol{\sigma} \rangle_{\Omega_1}$ is the average stress in the matrix phase and $\langle \boldsymbol{\sigma} \rangle_{\Omega}$ is the average stress over all phases. Using this result the material is then assumed to fail when the mean von Mises stress in the matrix phase is greater than the parameter σ_{mat}. In this case σ_{mat} is a parameter which includes any size dependent strengthening effects on the matrix material while the volume fraction and load sharing dependence is modeled through the stress concentration tensor.

In the first part of this paper, estimates are made for the extent of failed material due to a force acting on the surface of a micro or nanocomposite solid. This force is then used in a classical Boussinesq (mesoscopic) solution,

*Author to whom correspondence should be addressed.

however, using effective (homogenized) material properties. The stress concentration tensor and failure criteria described above are then used to determine the amount of failed material as a function of the volume fraction of the particulate phase and the material properties of each phase. In the second part of this work, the uncertainty in the homogenized properties of the composite is characterized by the width of the analytical Hashin-Shtrikman bounds. The width of these bounds accounts for uncertainties in factors such as the morphology of the particles and their distribution within the matrix material. The subsurface damage model derived in the first part of this paper is then used to quantify the uncertainty in the amount of damaged material as a function of the volume fraction of the particulate phase and of the individual material properties.

2. MICROMECHANICAL CHARACTERIZATION OF A HETEROGENEOUS SOLID

In this approach, the determination of the extent of damage of a solid possessing small second phase particles will require knowledge of the overall effective mechanical properties of micro or nano-heterogeneous materials, for example, comprised of particles suspended in a binding matrix (Fig. 1).

2.1. Effective Properties

In order to determine overall properties, we draw on results from the theory of heterogeneous solids. We denote by $\mathbb{E}^*$ the effective mechanical response (or stiffness), a fourth-order elasticity tensor, described via the relation between average stress and strain fields: $\langle \boldsymbol{\sigma} \rangle_\Omega = \mathbb{E}^* : \langle \boldsymbol{\epsilon} \rangle_\Omega$. Here $\langle \cdot \rangle_\Omega \stackrel{\text{def}}{=} (1/|\Omega|) \int_\Omega \cdot \, d\Omega$, and $\boldsymbol{\sigma}$ and $\boldsymbol{\epsilon}$ are the stress and strain tensor fields within a statistically representative volume element (RVE) of volume $|\Omega|$. We shall assume that the effective response $\mathbb{E}^*$ is isotropic, which is obtained when the particles are randomly distributed and randomly oriented. It can be shown that when the body is isotropic, there are only two independent constants in $\mathbb{E}^*$, which has the following action

$$\mathbb{E}^* : \langle \boldsymbol{\epsilon} \rangle_\Omega = 3\kappa^* \left\langle \frac{tr\boldsymbol{\epsilon}}{3} \right\rangle_\Omega \mathbf{1} + 2\mu^* \langle \boldsymbol{\epsilon}' \rangle_\Omega \tag{1}$$

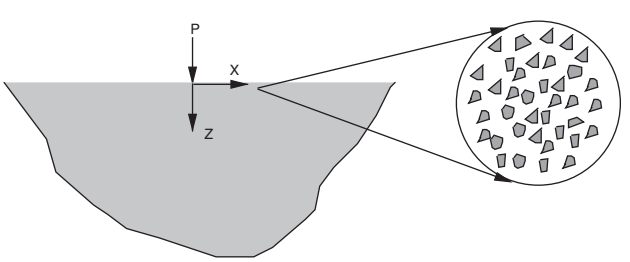

Fig. 1. Idealized loading on the surface of a heterogeneous material.

where the effective bulk and shear moduli are given by $3\kappa^* \stackrel{\text{def}}{=} \langle tr\boldsymbol{\sigma}/3 \rangle_\Omega / \langle tr\boldsymbol{\epsilon}/3 \rangle_\Omega$ and $2\mu^* \stackrel{\text{def}}{=} \sqrt{\langle \boldsymbol{\sigma}' \rangle_\Omega : \langle \boldsymbol{\sigma}' \rangle_\Omega / \langle \boldsymbol{\epsilon}' \rangle_\Omega : \langle \boldsymbol{\epsilon}' \rangle_\Omega}$, where $tr\boldsymbol{\epsilon} = \epsilon_{ii}$ and $\boldsymbol{\epsilon}' = \boldsymbol{\epsilon} - (1/3)(tr\boldsymbol{\epsilon})\mathbf{1}$ is the deviatoric strain. See Torquato[7–11] for details on effective properties.

Classical approaches have sought to approximate or bound effective responses. A widely used set of estimates for the effective properties are the Hashin-Shtrikman bounds,[12–13] for isotropic materials with isotropic effective responses. The Hashin-Shtrikman bounds for the bulk moduli are

$$\begin{aligned} \kappa^{*,-} &\stackrel{\text{def}}{=} \kappa_1 + \frac{v_2}{1/(\kappa_2 - \kappa_1) + (3(1-v_2))/(3\kappa_1 + 4\mu_1)} \\ &\leq \kappa^* \leq \kappa_2 + \frac{1 - v_2}{1/(\kappa_1 - \kappa_2) + (3v_2)/(3\kappa_2 + 4\mu_2)} \\ &\stackrel{\text{def}}{=} \kappa^{*,+} \end{aligned} \tag{2}$$

and for the shear moduli

$$\begin{aligned} \mu^{*,-} &\stackrel{\text{def}}{=} \mu_1 + \frac{v_2}{1/(\mu_2 - \mu_1) + (6(1-v_2)(\kappa_1 + 2\mu_1))/(5\mu_1(3\kappa_1 + 4\mu_1))} \\ &\leq \mu^* \leq \mu_2 + \frac{(1-v_2)}{1/(\mu_1 - \mu_2) + (6v_2(\kappa_2 + 2\mu_2))/(5\mu_2(3\kappa_2 + 4\mu_2))} \\ &\stackrel{\text{def}}{=} \mu^{*,+} \end{aligned} \tag{3}$$

where $\kappa_2 \geq \kappa_1$ are the bulk moduli and $\mu_2 \geq \mu_1$ are the shear moduli of the particle and binder phases respectively, and v_2 is the volume fraction of particles.[a] Such bounds are the tightest known on isotropic effective responses, with isotropic two phase microstructures, where only the volume fractions and phase contrasts of the constituents are known. Note that no further geometric information, such as the number and nature of particles, etc., contributes to these bounds.

2.2. Concentration Tensors

The load carried by each phase in the microstructure is characterized via concentration tensors, to which we now turn. These provide a measure of the deviation away from the mean fields throughout the material. One can decompose averages of an arbitrary quantity over Ω into averages over each of the phases in the following manner: $\langle \boldsymbol{A} \rangle_\Omega = (1/|\Omega|)(\int_{\Omega_1} \boldsymbol{A} \, d\Omega + \int_{\Omega_2} \boldsymbol{A} \, d\Omega) = v_1 \langle \boldsymbol{A} \rangle_{\Omega_1} + v_2 \langle \boldsymbol{A} \rangle_{\Omega_2}$, where the domain of the matrix phase is Ω_1 and the domain of the particle phase is Ω_2.

If we make use of this decomposition, we have

$$\begin{aligned} \langle \boldsymbol{\sigma} \rangle_\Omega &= v_1 \langle \boldsymbol{\sigma} \rangle_{\Omega_1} + v_2 \langle \boldsymbol{\sigma} \rangle_{\Omega_2} \\ &= v_1 \mathbb{E}_1 : \langle \boldsymbol{\epsilon} \rangle_{\Omega_1} + v_2 \mathbb{E}_2 : \langle \boldsymbol{\epsilon} \rangle_{\Omega_2} \\ &= \mathbb{E}_1 : (\langle \boldsymbol{\epsilon} \rangle_\Omega - v_2 \langle \boldsymbol{\epsilon} \rangle_{\Omega_2}) + v_2 \mathbb{E}_2 : \langle \boldsymbol{\epsilon} \rangle_{\Omega_2} \\ &= (\mathbb{E}_1 + v_2(\mathbb{E}_2 - \mathbb{E}_1) : \boldsymbol{C}) : \langle \boldsymbol{\epsilon} \rangle_\Omega \end{aligned} \tag{4}$$

[a]The volume fraction of the matrix is v_1, where $v_1 + v_2 = 1$.

where $\boldsymbol{C} \stackrel{\text{def}}{=} (1/v_2(\boldsymbol{IE}_2 - \boldsymbol{IE}_1)^{-1}\colon(\boldsymbol{IE}^* - \boldsymbol{IE}_1))$, with $\boldsymbol{C}\colon \langle\boldsymbol{\epsilon}\rangle_\Omega = \langle\boldsymbol{\epsilon}\rangle_{\Omega_2}$. The strain concentration tensor $\boldsymbol{C}$ relates the average strain over the particle phase (2) to the average strain over all phases. Similarly, for the variation in the stress we have $\boldsymbol{C}\colon \boldsymbol{IE}^{*-1}\colon \langle\boldsymbol{\sigma}\rangle_\Omega = \boldsymbol{IE}_2^{-1}\colon \langle\boldsymbol{\sigma}\rangle_{\Omega_2}$, which reduces to $\boldsymbol{IE}_2\colon \boldsymbol{C}\colon \boldsymbol{IE}^{*-1}\colon \langle\boldsymbol{\sigma}\rangle_\Omega \stackrel{\text{def}}{=} \bar{\boldsymbol{C}}\colon \langle\boldsymbol{\sigma}\rangle_\Omega = \langle\boldsymbol{\sigma}\rangle_{\Omega_2} \cdot \bar{\boldsymbol{C}}$ is known as the stress concentration tensor; it relates the average stress in the particle phase to that in the whole RVE. Note that once either $\bar{\boldsymbol{C}}$ or $\boldsymbol{IE}^*$ are known, the other can be determined. In the case of isotropy we may write

$$\bar{C}_\kappa \stackrel{\text{def}}{=} \frac{1}{v_2}\frac{\kappa_2}{\kappa^*}\frac{\kappa^* - \kappa_1}{\kappa_2 - \kappa_1} \quad \text{and} \quad \bar{C}_\mu \stackrel{\text{def}}{=} \frac{1}{v_2}\frac{\mu_2}{\mu^*}\frac{\mu^* - \mu_1}{\mu_2 - \mu_1} \tag{5}$$

where $\bar{C}_\kappa\langle tr\boldsymbol{\sigma}/3\rangle_\Omega = \langle tr\boldsymbol{\sigma}/3\rangle_{\Omega_2}$ and where $\bar{C}_\mu\langle\boldsymbol{\sigma}'\rangle_\Omega = \langle\boldsymbol{\sigma}'\rangle_{\Omega_2}$. Clearly, the microstress fields are minimally distorted when $\bar{C}_\kappa = \bar{C}_\mu = 1$; there are no stress concentrations in a homogeneous material. For the matrix,

$$\begin{aligned}\langle\boldsymbol{\sigma}\rangle_{\Omega_1} &= \frac{\langle\boldsymbol{\sigma}\rangle_\Omega - v_2\langle\boldsymbol{\sigma}\rangle_{\Omega_2}}{v_1} = \frac{\langle\boldsymbol{\sigma}\rangle_\Omega - v_2\bar{\boldsymbol{C}}\colon\langle\boldsymbol{\sigma}\rangle_\Omega}{v_1} \\ &= \frac{(\boldsymbol{1} - v_2\bar{\boldsymbol{C}})\colon\langle\boldsymbol{\sigma}\rangle_\Omega}{v_1} \stackrel{\text{def}}{=} \bar{\bar{\boldsymbol{C}}}\colon\langle\boldsymbol{\sigma}\rangle_\Omega\end{aligned} \tag{6}$$

Therefore, in the case of isotropy,

$$\bar{\bar{C}}_\kappa \stackrel{\text{def}}{=} \frac{1}{v_1}(1 - v_2\bar{C}_\kappa) \quad \text{and} \quad \bar{\bar{C}}_\mu \stackrel{\text{def}}{=} \frac{1}{v_1}(1 - v_2\bar{C}_\mu) \tag{7}$$

The utility of such relations is that they allow one to determine what the load sharing is for each phase. Typically, we are interested in the failure of the matrix that binds the particulates together.

3. FAILURE ENVELOPES

The classical, mesoscopic, Boussinesq[14] problem of a static normal point force on an infinite half space, whose symmetric, θ-independent solution is, in polar coordinates, to provide the macroscale stress field

$$\begin{aligned}\langle\sigma_{rr}\rangle_\Omega &= \frac{P}{2\pi}\left((1-2\nu^*)\left(\frac{1}{r^2} - \frac{z}{\gamma r^2}\right) - \frac{3zr^2}{\gamma^5}\right) \\ \langle\sigma_{\theta\theta}\rangle_\Omega &= -\frac{P}{2\pi}(1-2\nu^*)\left(\frac{1}{r^2} - \frac{z}{\gamma r^2} - \frac{z}{\gamma^3}\right) \\ \langle\sigma_{zz}\rangle_\Omega &= -\frac{3P}{2\pi}\frac{z^3}{\gamma^5} \\ \langle\sigma_{rz}\rangle_\Omega &= -\frac{3P}{2\pi}\frac{rz^2}{\gamma^5} \\ \langle\sigma_{r\theta}\rangle_\Omega &= 0 \quad \text{(symmetry)} \\ \langle\sigma_{z\theta}\rangle_\Omega &= 0 \quad \text{(symmetry)}\end{aligned} \tag{8}$$

where $r \stackrel{\text{def}}{=} \sqrt{x^2 + y^2}$ and $\gamma \stackrel{\text{def}}{=} \sqrt{x^2 + y^2 + z^2}$ and where the effective Poisson ratio is given by

$$\nu^* = \frac{3\kappa^* - 2\mu^*}{2(3\kappa^* + \mu^*)} \tag{9}$$

It is convenient to employ Cartesian bases in the rest of the analysis. Due to the symmetry of the problem we may write, letting $x = r$, $y = 0$, $\langle\sigma_{xx}\rangle_\Omega = \langle\sigma_{rr}\rangle_\Omega$, $\langle\sigma_{yy}\rangle_\Omega = \langle\sigma_{\theta\theta}\rangle_\Omega$, $\langle\sigma_{xz}\rangle_\Omega = \langle\sigma_{rz}\rangle_\Omega$ and due to symmetry $\langle\sigma_{yz}\rangle_\Omega = 0$ and $\langle\sigma_{xy}\rangle_\Omega = 0$. Since this solution is independent of θ, thus if it is valid for a point where $x = r$, $y = 0$, it is valid for any other point with the same value of r, provided the z coordinates are the same. Essentially, the problem is two-dimensional.

From Eqs. (7) and (8) one can determine all points which satisfy the von Mises failure criteria *for the matrix material*

$$\langle\boldsymbol{\sigma}'\rangle_{\Omega_1} : \langle\boldsymbol{\sigma}'\rangle_{\Omega_1} = (\bar{\bar{C}}_\mu)^2\langle\boldsymbol{\sigma}'\rangle_\Omega\colon\langle\boldsymbol{\sigma}'\rangle_\Omega \geq \frac{2}{3}\sigma_{\text{mat}}^2 \tag{10}$$

which correspond to failed material locations, where σ_{mat} is a critical stress for matrix failure. More explicitly, one may write

$$\underbrace{(\langle\sigma_{rr}\rangle_\Omega - \langle\sigma_{\theta\theta}\rangle_\Omega)^2 + (\langle\sigma_{\theta\theta}\rangle_\Omega - \langle\sigma_{zz}\rangle_\Omega)^2 + (\langle\sigma_{zz}\rangle_\Omega - \langle\sigma_{rr}\rangle_\Omega)^2 + 6(\langle\sigma_{rz}\rangle_\Omega)^2}_{\text{depends on } v_2 \text{ through } \nu^*} \geq \underbrace{\frac{2}{(\bar{\bar{C}}_\mu)^2}\sigma_{\text{mat}}^2}_{\text{depends on } v_2 \text{ through } \bar{\bar{C}}_\mu} \tag{11}$$

Figure 2 shows a sample calculation using the material properties given in Table I and $P = 50$ mN.

A straightforward estimate of the effective properties is to take a convex combination of the bounds, for example,

$$\begin{aligned}\kappa^* &\approx \phi\kappa^{*,+} + (1-\phi)\kappa^{*,-} \quad \text{and} \\ \mu^* &\approx \phi\mu^{*,+} + (1-\phi)\mu^{*,-}\end{aligned} \tag{12}$$

where $0 \leq \phi \leq 1$. Essentially, for microstructures comprised of hard particles surrounded by a continuous soft matrix, which produces an overall stiffness that is significantly smaller than the reverse, a hard matrix encasing soft particles, it is well-known that the Hashin-Shtrikman lower bound is quite accurate (Hashin[15]). For this example and for the parameter studies in the following section we use $\phi = 0.25$. Figures 2(a) and (b) show the shape of the damage profile and the corresponding volume encapsulated by the profile as a function of the volume fraction of the particulate material. From Eqs. (8) and (11), it is clear that these profiles are a function of ν^* and $\bar{\bar{C}}_\mu$. Figures 2(b) and (c) show how ν^* and $\bar{\bar{C}}_\mu$ vary as a function of v_2. Usually, only small volume fractions of particles are of practical interest, however, in this example v_2 is plotted over its entire range for completeness.

4. PARAMETER STUDIES

It was seen in the previous section that the volume of damaged material depends on the effective Poisson ratio

RESEARCH ARTICLE

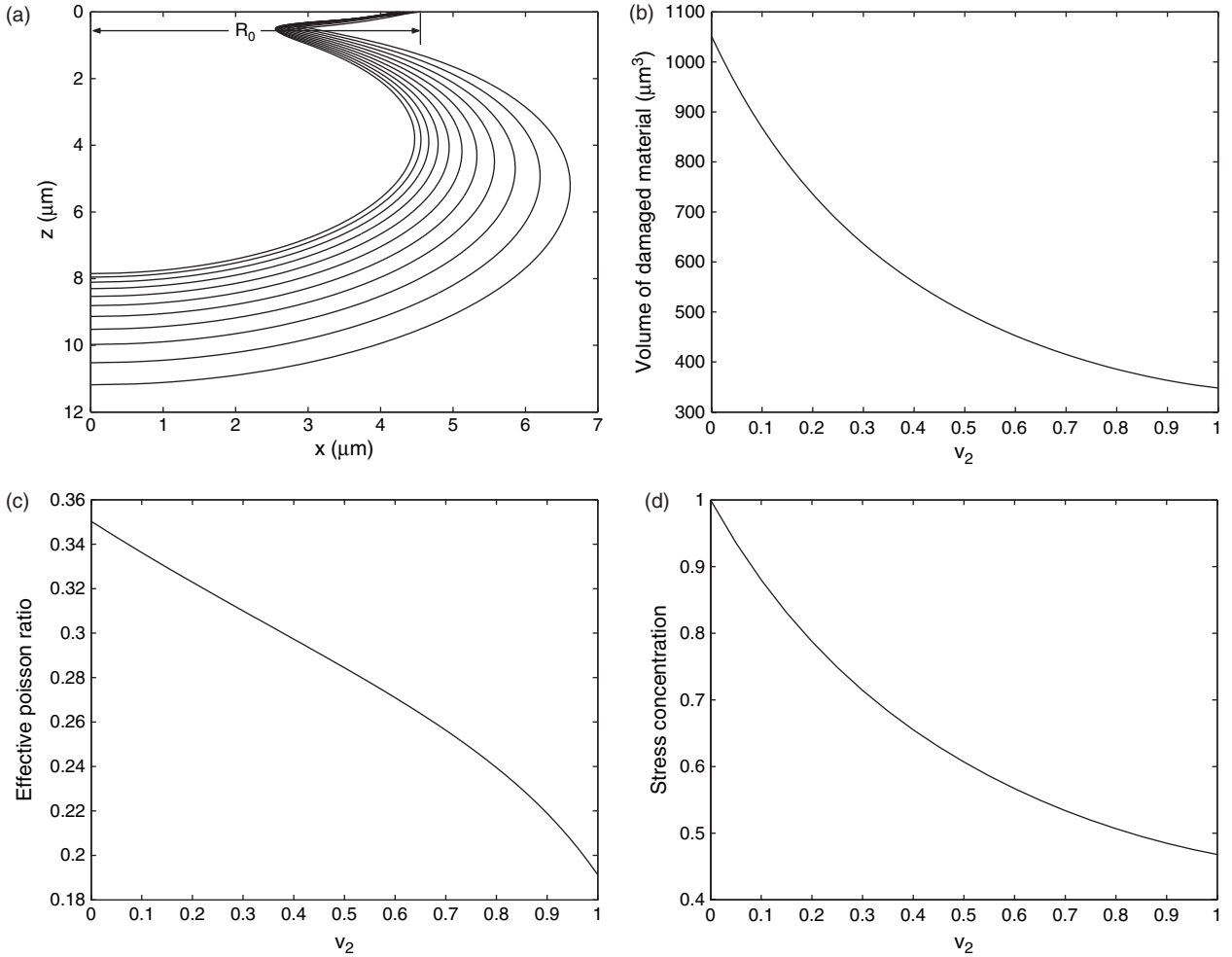

Fig. 2. (a) The profile (one quarter) of the damaged material boundary underneath a concentrated load for $P = 50$ mN as a function of v_2 and (b) the corresponding volume of damaged material. (c) The effective Poisson ratio as a function of particulate volume fraction. (d) The shear concentration function for the matrix material as a function of particulate volume fraction.

and the stress concentration factor. In the first part of this section, the behavior of the volume of damaged material with respect to ν^* and $\bar{\bar{C}}_\mu$ is investigated, and a decomposition of the amount of volume damaged is made in terms of independent functions of ν^* and $\bar{\bar{C}}_\mu$. In the second part of this section, the sensitivity of the subsurface damage model to the bulk and shear modulus mismatch ratios and the volume fraction of the particulate phase is examined. The bulk modulus mismatch ratio, r_κ, and shear modulus mismatch ratio, r_μ, are defined as

$$r_\kappa \stackrel{\text{def}}{=} \frac{\kappa_2}{\kappa_1} \quad \text{and} \quad r_\mu \stackrel{\text{def}}{=} \frac{\mu_2}{\mu_1} \tag{13}$$

In the remaining parts of this paper, the properties given in Table I are used for the matrix material, while the properties of the particulate phase are set by the mismatch ratio.

For $z = 0$, one finds that the radial distance to the edge of the failure envelope is

$$R_0 = \left[\frac{\sqrt{3}P(1-2\nu^*)\bar{\bar{C}}_\mu}{2\pi\sigma_{\text{mat}}}\right]^{1/2} \tag{14}$$

Figure 2(a) shows R_0 for the largest failure envelope in this plot. From this result, it is plausible to expect that the volume of damaged material depends approximately on R_0^3, thus it would depend on $\bar{\bar{C}}_\mu^{3/2}$. Figure 3 shows the dependence of the volume of damaged material on the Poisson ratio and the shear concentration factor. Plot (a) shows the volume of damaged material for different values of $\bar{\bar{C}}_\mu^{3/2}$, and plot (b) shows the ratio of the volume damaged to $\bar{\bar{C}}_\mu^{3/2}$ as a function of $\bar{\bar{C}}_\mu$. From this plot, it can be seen that

Table I. Material properties used for the model problem.

Material property	Value
κ_1 (GPa)	77.9
μ_1 (GPa)	25.9
κ_2 (GPa)	230
μ_2 (GPa)	172
σ_{mat} (MPa)	200

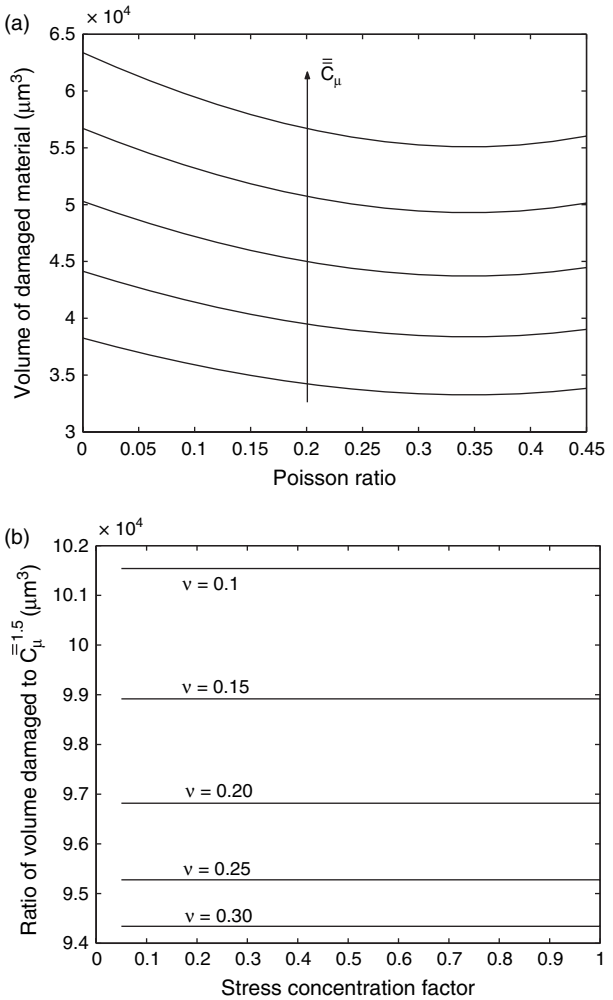

Fig. 3. (a) The volume of damaged material as a function of the Poisson ratio and (b) the ratio of volume damaged to $\bar{\bar{C}}_\mu^{3/2}$ as a function of the shear concentration factor for the matrix material.

$v_{\text{damaged}}/\bar{\bar{C}}_\mu^{3/2}$ is independent of $\bar{\bar{C}}_\mu$ and, therefore, only a function of ν^*. From Eqs. (8) and (11), it can be seen that the damage profile has the same functional dependence on $\bar{\bar{C}}_\mu$ as it does on $P\bar{\bar{C}}_\mu/\sigma_{\text{mat}}$. Using these observations, the volume of damaged material can be expresses as

$$v_{\text{damaged}} = g(\nu^*)\left(\frac{P\bar{\bar{C}}_\mu}{\sigma_{\text{mat}}}\right)^{3/2} \tag{15}$$

where $g(\nu^*)$ is a function of the Poisson ratio which is shown in Figure 4. Note that $g(\nu^*)$ has a minimum value for $\nu^* \approx 0.35$.

Figure 5 shows how the volume of damaged material depends on the particulate volume fraction, the shear modulus mismatch ratio, and the bulk modulus mismatch ratio. From plot (a) of this figure, the following observations are made:

- The amount of damaged volume is more sensitive to changes in r_μ than to changes in r_κ.

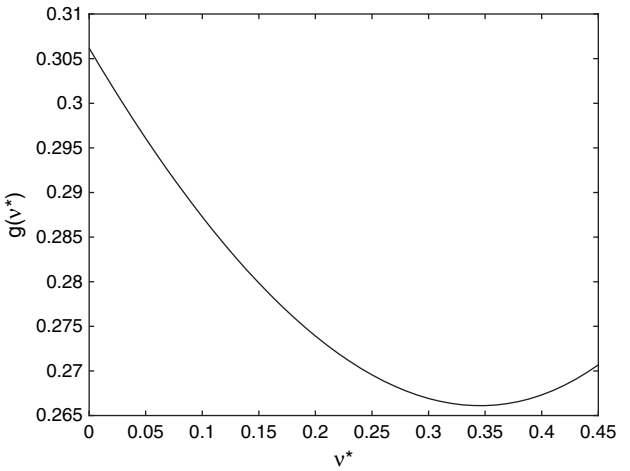

Fig. 4. Plot of $g(\nu^*)$ where $v_{\text{damaged}} = g(\nu^*)(P\bar{\bar{C}}_\mu/\sigma_{\text{mat}})^{3/2}$.

- For small values of r_μ, the amount of damaged volume is nearly insensitive to changes in r_κ.
- For higher values of r_μ, v_{damaged} is more sensitive to changes in r_κ when r_κ is small and less sensitive to changes in r_κ when r_κ is large.

Since it is apparent that r_μ is more important than r_κ in the sensitivity of the volume of damaged material, Figure 5(b) shows a plot of v_{damaged} as a function of r_μ. From this plot, the following observations are made:

- v_{damaged} is not highly sensitive to changes in r_μ for small volume fractions.
- v_{damaged} is more sensitive to changes in r_μ for lower values of r_μ.

5. UNCERTAINTY QUANTIFICATION

In this section the effect of the uncertainty in κ^* and μ^* on the uncertainty in the volume of the damaged material is examined. Using Eqs. (2) and (3), the bounds on κ^* and μ^* are determined such that $\kappa^{*,-} \leq \kappa^* \leq \kappa^{*,+}$ and $\mu^{*,-} \leq \mu^* \leq \mu^{*,+}$. In this analysis, it is assumed that all values of κ^* and μ^* within the given bounds are equally likely. Therefore, a uniform distribution is used to describe κ^* and μ^*. The fractional uncertainties in κ^* and μ^* are defined as $\delta\kappa^*/\kappa^* \stackrel{\text{def}}{=} (\kappa^{*,+} - \kappa^{*,-})/(\kappa^{*,+} + \kappa^{*,-})$ and $\delta\mu^*/\mu^* \stackrel{\text{def}}{=} (\mu^{*,+} - \mu^{*,-})/(\mu^{*,+} + \mu^{*,-})$ respectively.

Figure 6 shows the fractional uncertainty in κ^* and μ^* as a function of r_κ and r_μ for $v_2 = 0.01$. From this figure, the following is observed:

- The uncertainties in κ^* and μ^* increase as r_κ and r_μ increase.
- The uncertainty in κ^* is strongly dependent on both the bulk modulus and shear modulus mismatch ratios.
- The uncertainty in μ^* is strongly dependent on the shear modulus mismatch ratio and weakly dependent on the bulk modulus mismatch ratio.

RESEARCH ARTICLE

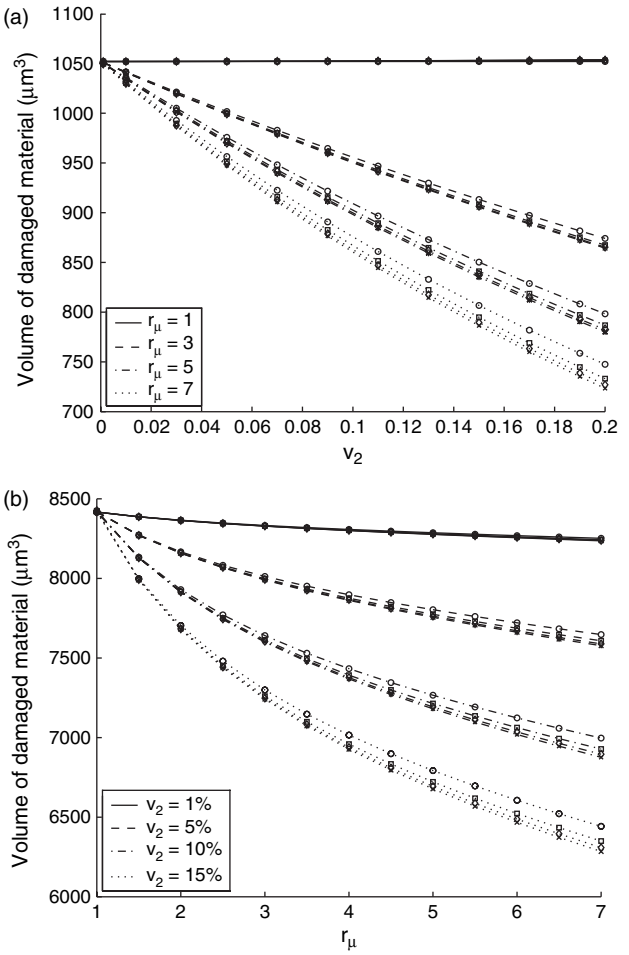

Fig. 5. Volume of damaged material as a function of (a) particulate volume fraction and (b) shear modulus mismatch ratio ($\circ$ $r_\kappa = 1$, $\square$ $r_\kappa = 3$, $\diamond$ $r_\kappa = 5$, $\times$ $r_\kappa = 7$).

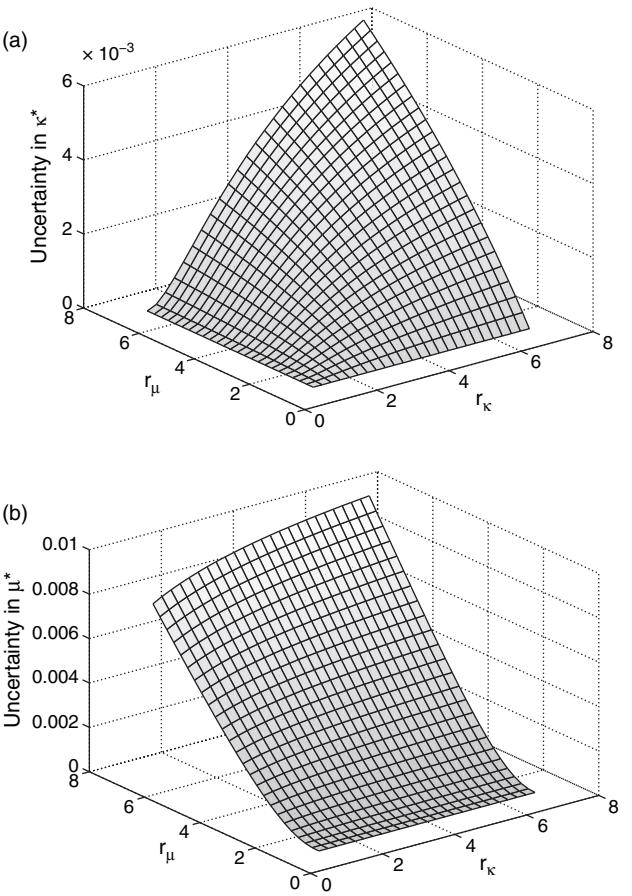

Fig. 6. Fractional uncertainty in (a) κ^* and (b) μ^* as a function of r_κ and r_μ for $v_2 = 0.01$.

Figure 7(a) shows how the uncertainty in κ^* varies as a function of v_2 for various values of r_κ and r_μ. For the range of v_2 shown in this figure, the following observations are made:[b]

- The uncertainties in κ^* and μ^* increase as v_2 increases.
- The uncertainties in κ^* and μ^* increase more rapidly for lower values of v_2 and less rapidly as v_2 increases further.
- The uncertainty in κ^* is strongly dependent on both r_κ and r_μ.
- The uncertainty in μ^* is is more sensitive to changes in r_μ than to changes in r_κ.

Equation (15) shows that the volume of damaged material depends on κ^* and μ^* through the effective Poisson ratio, ν^*, and $\bar{\bar{C}}_\mu$. In fact, only ν^* depends on both κ^* and μ^* since $\bar{\bar{C}}_\mu$ only depends on μ^*. Given that κ^* and μ^* are assumed to be uniformly distributed, it is of interest to determine the distribution of ν^* and $\bar{\bar{C}}_\mu$. If $\nu(\kappa^{*,+}, \mu^{*,+}) \geq \nu(\kappa^{*,-}, \mu^{*,-})$, then the probability density function for ν^* is given by

$$f_{\nu^*}(\nu^*) = \frac{1}{\Delta\mu^*\Delta\kappa^*} \begin{cases} \left(\dfrac{\mu^{*,+}}{1-2\nu^*}\right)^2 - \dfrac{9}{4}\left(\dfrac{\kappa^{*,-}}{1+\nu^*}\right)^2 \\ \quad \text{for } \nu(\kappa^{*,-}, \mu^{*,+}) \leq \nu^* \leq \nu(\kappa^{*,-}, \mu^{*,-}) \\ 2\dfrac{\mu^{*,-}\Delta\mu^*}{(1-2\nu^*)^2} + \left(\dfrac{\Delta\mu^*}{1-2\nu^*}\right)^2 \\ \quad \text{for } \nu(\kappa^{*,-}, \mu^{*,-}) \leq \nu^* \leq \nu(\kappa^{*,+}, \mu^{*,+}) \\ \dfrac{9}{4}\left(\dfrac{\kappa^{*,+}}{1+\nu^*}\right)^2 - \left(\dfrac{\mu^{*,-}}{1-2\nu^*}\right)^2 \\ \quad \text{for } \nu(\kappa^{*,+}, \mu^{*,+}) \leq \nu^* \leq \nu(\kappa^{*,+}, \mu^{*,-}) \\ 0 \quad \text{elsewhere} \end{cases} \tag{16}$$

where $\Delta\mu^* = \mu^{*,+} - \mu^{*,-}$, $\Delta\kappa^* = \kappa^{*,+} - \kappa^{*,-}$, and $\nu(\kappa, \mu)$ is evaluated using Eq. (9). If $\nu(\kappa^{*,+}, \mu^{*,+}) \leq \nu(\kappa^{*,-}, \mu^{*,-})$, then

[b]Note that for $v_2 = 0$ and $v_2 = 1$ the uncertainty vanishes; therefore, if v_2 were increased further in Figure 7, the uncertainty would eventually decrease with increasing v_2.

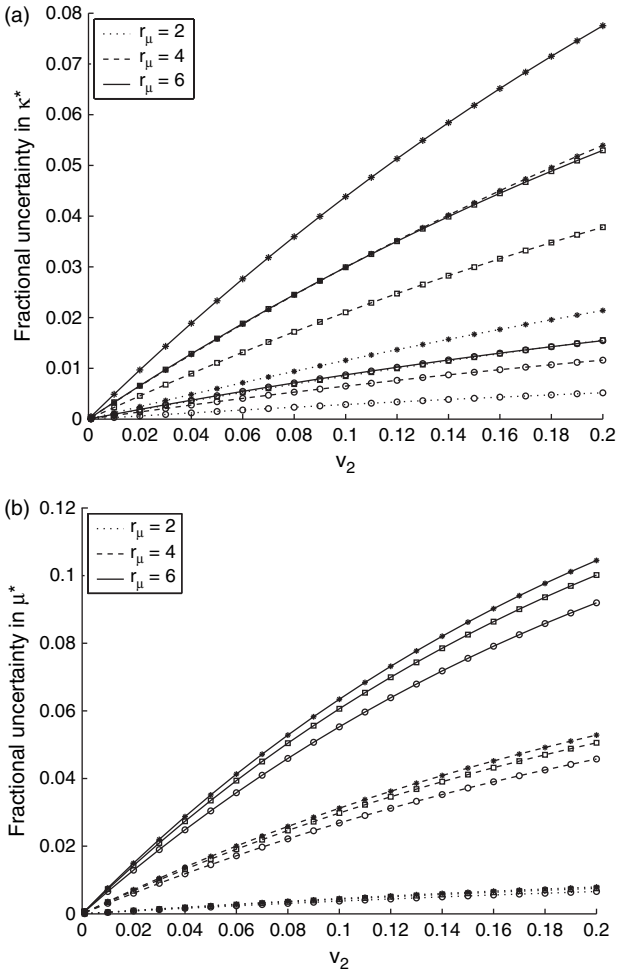

Fig. 7. Fractional uncertainty in (a) κ^* and (b) μ^* as a function of v_2 ($\circ$ $r_\kappa = 2$, $\square$ $r_\kappa = 4$, * $r_\kappa = 6$).

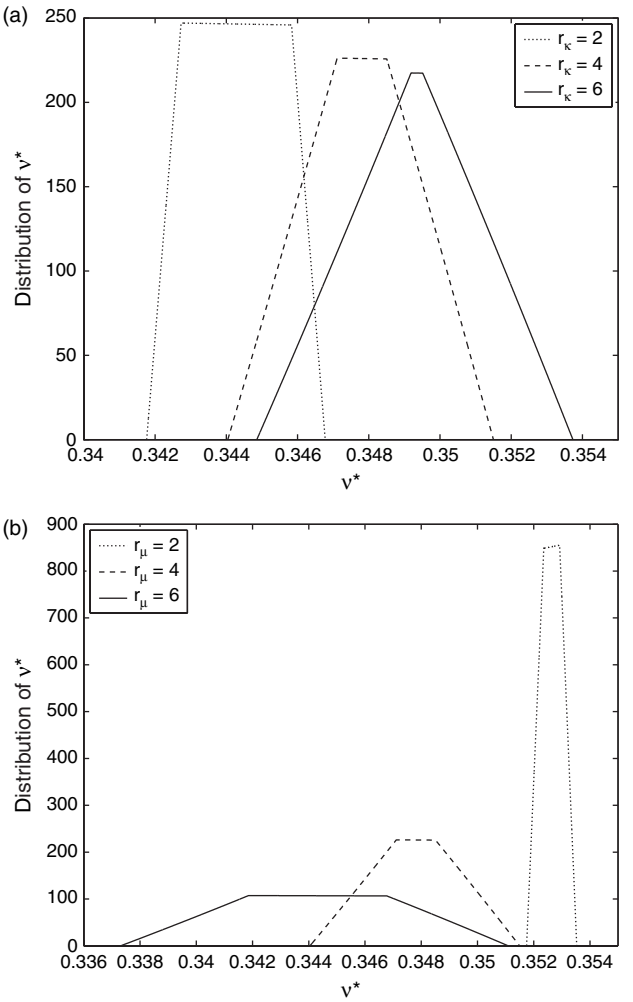

Fig. 8. Probability density function of the effective Poisson ratio as a function of (a) the bulk modulus mismatch ratio and (b) the shear modulus mismatch ratio. The width of the distribution corresponds to the uncertainty in the effective Poisson ratio. From the plots it is seen that the uncertainty in ν^* is more sensitive to variations in r_μ than to variations in r_κ.

$$f_{\nu^*}(\nu^*) = \frac{1}{\Delta\mu^*\Delta\kappa^*} \begin{cases} \left(\dfrac{\mu^{*,+}}{1-2\nu^*}\right)^2 - \dfrac{9}{4}\left(\dfrac{\kappa^{*,-}}{1+\nu^*}\right)^2 \\ \quad \text{for } \nu(\kappa^{*,-},\mu^{*,+}) \le \nu^* \le \nu(\kappa^{*,+},\mu^{*,+}) \\ \dfrac{9}{2}\dfrac{\kappa^{*,+}\Delta\kappa^*}{(1+\nu^*)^2} - \dfrac{9}{4}\left(\dfrac{\Delta\kappa^*}{1+\nu^*}\right)^2 \\ \quad \text{for } \nu(\kappa^{*,+},\mu^{*,+}) \le \nu^* \le \nu(\kappa^{*,-},\mu^{*,-}) \\ \dfrac{9}{4}\left(\dfrac{\kappa^{*,+}}{1+\nu^*}\right)^2 - \left(\dfrac{\mu^{*,-}}{1-2\nu^*}\right)^2 \\ \quad \text{for } \nu(\kappa^{*,-},\mu^{*,-}) \le \nu^* \le \nu(\kappa^{*,+},\mu^{*,-}) \\ 0 \quad \text{elsewhere} \end{cases} \tag{17}$$

Figure 8 shows the probability density function for ν^* for various values of r_κ and r_μ and $v_2 = 0.05$. In plot (a) the distribution of ν^* is shown for $r_\mu = 4$ and $r_\kappa = 2$, 4, and 6, and in plot (b) the distribution of ν^* is shown for $r_\kappa = 4$ and $r_\mu = 2$, 4, and 6. From this figure, the following is observed:

- As r_κ increases, the width of the distribution of ν^* increases. This is expected since the uncertainties in κ^* and to a lesser extent in μ^* increase as r_κ increases.
- As r_μ increases, the width of the distribution of ν^* also increases, and the increase is greater than when r_κ is varied. This occurs because the uncertainties in both κ^* and μ^* are highly sensitive to changes in r_μ.
- For the model problem considered here, the range of effective Poisson ratios varies from approximately 0.336 to approximately 0.354 for r_κ and r_μ ranging from 2 to 6. Note that for these values of ν^*, $g(\nu^*)$ is fairly insensitive to variations in ν^*.

The probability density function for $\bar{\bar{C}}_\mu$ is given by

$$f_{\bar{\bar{C}}_\mu}(\bar{\bar{C}}_\mu) = \frac{1}{\Delta\mu^*}\begin{cases} \dfrac{1}{\mu_2-\mu_1}\dfrac{\mu_1\mu_2 v_1}{(v_1\bar{\bar{C}}_\mu+(\mu_2/(\mu_2-\mu_1))-1)^2} \\ \quad \text{for } \bar{\bar{C}}_\mu(\mu^{*,+}) \le \bar{\bar{C}}_\mu \le \bar{\bar{C}}_\mu(\mu^{*,-}) \\ 0 \quad \text{elsewhere} \end{cases} \tag{18}$$

where $\bar{\bar{C}}_\mu(\mu^{*,+})$ and $\bar{\bar{C}}_\mu(\mu^{*,-})$ correspond to $\bar{\bar{C}}_\mu$ evaluated at $\mu^* = \mu^{*,+}$ and $\mu^* = \mu^{*,-}$ respectively. Figure 9 shows the probability density function for $\bar{\bar{C}}_\mu$ for various values of r_κ and r_μ and $v_2 = 0.05$. Although $\bar{\bar{C}}_\mu$ only depends on μ^*, since μ^* depends on both r_κ and r_μ then $\bar{\bar{C}}_\mu$ is also a function of r_κ. In plot (a) the distribution of $\bar{\bar{C}}_\mu$ is shown for $r_\mu = 4$ and $r_\kappa = 2$, 4, and 6, and in plot (b) the distribution of $\bar{\bar{C}}_\mu$ is shown for $r_\kappa = 4$ and $r_\mu = 2$, 4, and 6. From this figure, the following is observed:

- The distribution of $\bar{\bar{C}}_\mu$ is nearly insensitive to variations in r_κ. This can be seen from Eq. (18), where $f_{\bar{\bar{C}}_\mu}(\bar{\bar{C}}_\mu)$ only depends on r_κ through $\Delta\mu^*$ and $\bar{\bar{C}}_\mu$, which are not strongly dependent on r_κ.
- The distribution of $\bar{\bar{C}}_\mu$ is highly sensitive to variations in r_μ since $f_{\bar{\bar{C}}_\mu}(\bar{\bar{C}}_\mu)$ is explicitly a function of r_μ. As r_μ increases, the width of the distribution of $\bar{\bar{C}}_\mu$ increases.

For the purpose of comparison, the probability density functions of ν^* and $\bar{\bar{C}}_\mu$ are shown if Figure 10 for both the deterministic approach and a Monte-Carlo approach. For the Monte-Carlo approach, random values of μ^* and κ^* are chosen within the predicted bounds for the given set of input parameters. The values of ν^* or $\bar{\bar{C}}_\mu$ are then computed in terms of μ^* and κ^*. This process is repeated N_{mc} times to determine the probability density functions for ν^* or $\bar{\bar{C}}_\mu$. From Figure 10, it is clear that both the deterministic and Monte-Carlo approaches give the same

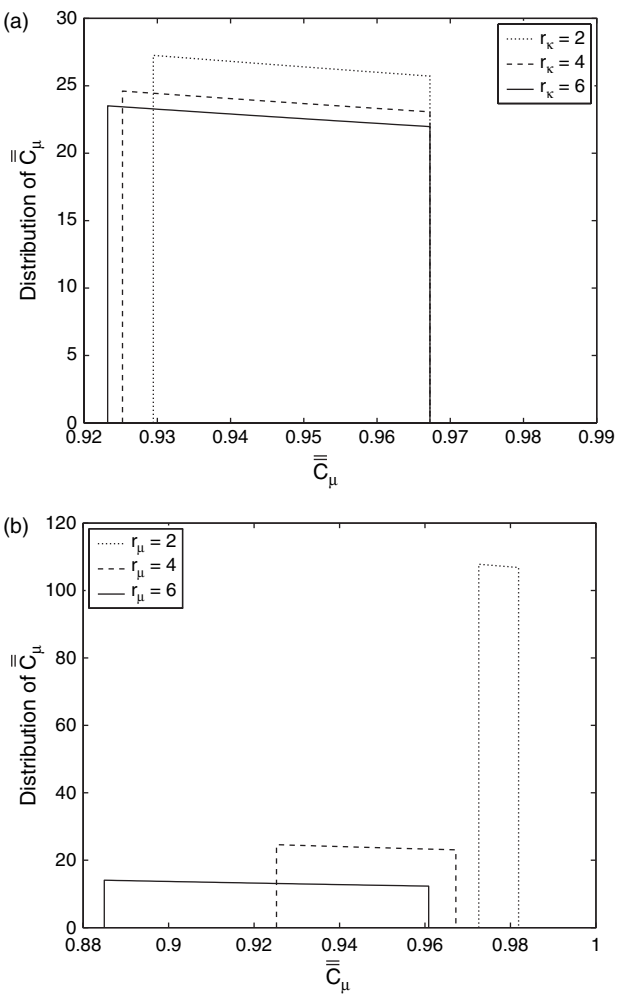

Fig. 9. Probability density function of $\bar{\bar{C}}_\mu$ as a function of (a) the bulk modulus mismatch ratio and (b) the shear modulus mismatch ratio. The width of the distribution corresponds to the uncertainty in $\bar{\bar{C}}_\mu$. From the plots it is seen that the uncertainty in $\bar{\bar{C}}_\mu$ highly sensitive to variations in r_μ and and nearly insensitive to variations in r_κ.

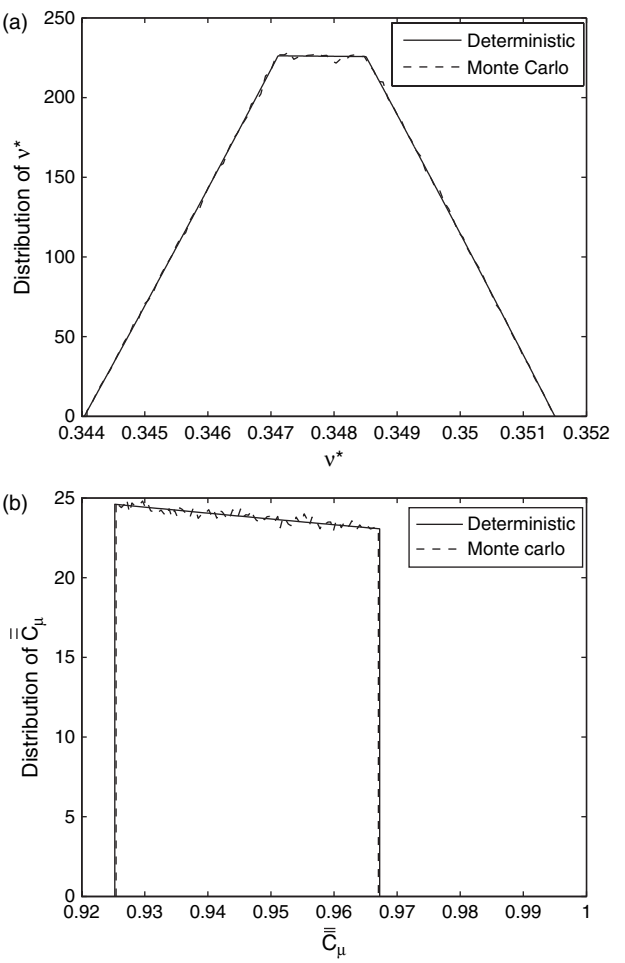

Fig. 10. Comparison of the probability density functions for the deterministic and Monte-Carlo approaches for (a) ν^* and (b) $\bar{\bar{C}}_\mu$. For both cases the mismatch ratios are $r_\mu = 4$ and $r_\kappa = 4$.

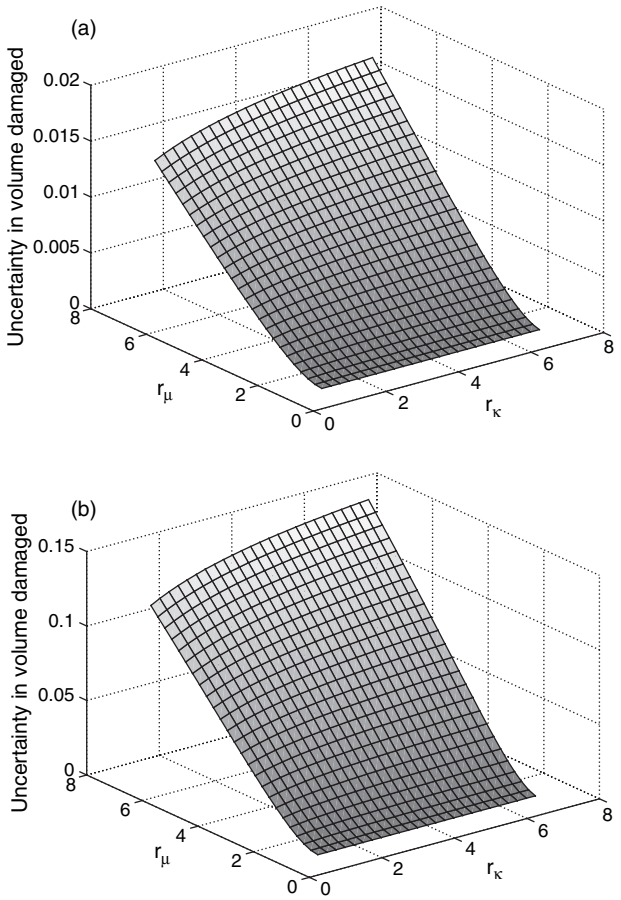

Fig. 11. Fractional uncertainty of the volume of damaged material as a function of the mismatch ratios for (a) $v_2 = 0.01$ and (b) $v_2 = 0.10$.

results. The distribution of ν^* and $\bar{\bar{C}}_\mu$ provide insight into the effect that the uncertainty in κ^* and μ^* have on the volume of damaged material.

The uncertainty in the volume of damaged material is computed only using the Monte-Carlo approach

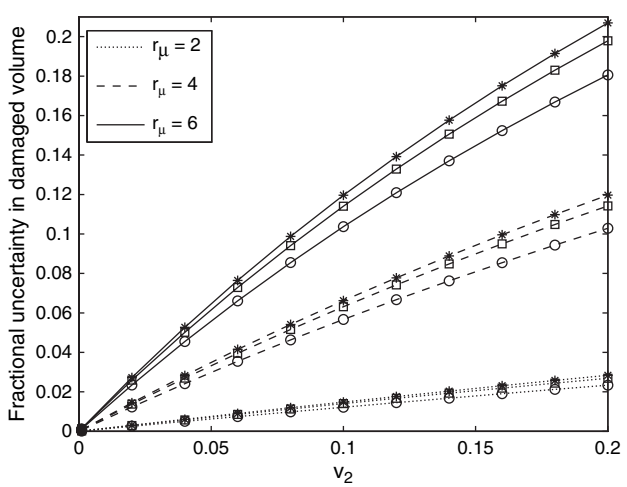

Fig. 12. Fractional uncertainty of the volume of damaged material as a function of v_2 ($\circ$ $r_\kappa = 2$, $\square$ $r_\kappa = 4$, $*$ $r_\kappa = 6$).

that was described in the previous paragraph. The fractional uncertainty in the volume of damaged material is defined as $\delta v_{\text{damaged}}/v_{\text{damaged}} = (v^+_{\text{damaged}} - v^-_{\text{damaged}})/(v^+_{\text{damaged}} + v^-_{\text{damaged}})$, where v^+_{damaged} and v^-_{damaged} are the maximum and minimum volume of damaged material from the Monte-Carlo simulation. Figure 11 shows the fractional uncertainty in the volume of damaged material as a function of the mismatch ratios for $v_2 = 0.01$ and $v_2 = 0.10$. From this figure, the following is observed:

- The uncertainty in the volume of damaged material increases as r_κ and r_μ increase. This is expected since the uncertainty in κ^* and μ^* increases as r_κ and r_μ increase.
- The uncertainty in the volume of damaged material is strongly dependent on the shear modulus mismatch ratio and weakly dependent on the bulk modulus mismatch ratio.

These are the same trends that are seen in the uncertainty of the effective shear modulus. Figure 12 shows how

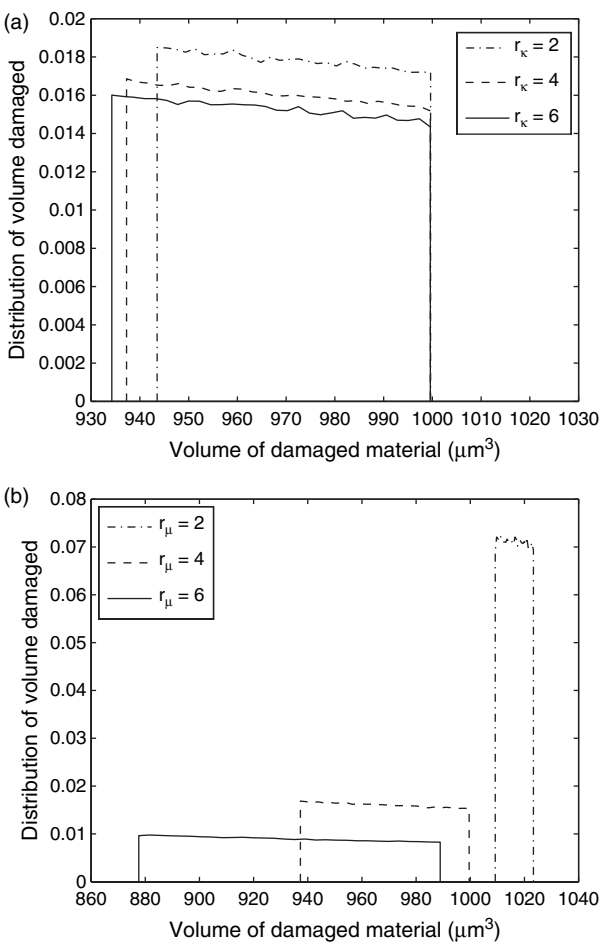

Fig. 13. Probability density function of v_{damaged} as a function of (a) the bulk modulus mismatch ratio and (b) the shear modulus mismatch ratio. The width of the distribution corresponds to the uncertainty in the volume of damaged material. Comparing this figure with Figure 9 clearly shows that the uncertainty in the amount of damaged material is mainly dependent on the uncertainty in the stress concentration factor.

the fractional uncertainty of the volume of damaged material varies as a function of v_2. For the range of volume fractions shown in this figure, the following observations are made:

- The uncertainty in the volume of damaged material increases as v_2 increases. This is expected since the uncertainty in κ^* and μ^* increases as v_2 increases.
- The uncertainty in the volume of damaged material increases more rapidly for lower values of v_2 and less rapidly as v_2 increases further. This is the same trend that was seen for the uncertainty in κ^* and μ^* as a function of v_2.

Figure 13 shows the distribution of the volume of damaged material from the Monte-Carlo simulation. Plot (a) shows this distribution for $v = 0.05$, $r_\mu = 4$, and $r_\kappa = 2$, 4, and 6, and plot (b) shows the distribution for for $r_\kappa = 4$ and $r_\mu = 2$, 4, and 6. From this figure it is observed that the distributions of v_{damaged} and $\bar{\bar{C}}_\mu$ show the same trends. Clearly, the uncertainty in the volume of damaged material is mainly dependent on the uncertainty in $\bar{\bar{C}}_\mu$. This is expected since for the values of ν^* shown in Figure 8, $g(\nu^*)$ is nearly insensitive to changes in ν^*. This can be seen from Figure 4 since the variation in $g(\nu^*)$ is small near the minimum of this function ($\nu^* \approx 0.35$).

6. DISCUSSION AND SUMMARY

In this work a micromechanical model for subsurface damage of micro and nanocomposites is developed. Parameter studies show that the model is highly sensitive to changes in the volume fraction of particulates and the shear modulus mismatch ratio and relatively insensitive to changes in the bulk modulus mismatch ratio. The uncertainty in the amount of volume damaged with respect to the uncertainty in the effective properties of the material is also examined in this paper. It is found that the uncertainty in the amount of subsurface volume damaged is strongly dependent on the stress concentration factor and weakly dependent on the effective Poisson ratio. The stress concentration factor is more sensitive to changes in the shear modulus mismatch ratio than to changes in the bulk modulus mismatch ratio; therefore, the uncertainty in the amount of material damaged is also more sensitive to the shear modulus mismatch ratio.

The matrix material is assumed to fail when the mean von Mises stress in the matrix phase exceeds σ_{mat}. The parameter σ_{mat} is the modified yield strength of the matrix material which accounts for particle size effects. In this work, these effects were not modeled explicitly. Zhang and Chen[16] have developed a model that includes the effects of particle size on the strength of the composite by taking into account the Orowan strengthening effect and enhanced dislocation density due to residual strains caused by thermal mismatch. In this work, it was assumed that there was no uncertainty in σ_{mat}. However, since for small particles σ_{mat} is dependent on particle size, it is clear that uncertainties in particle size and particle size distribution will lead to uncertainty in σ_{mat}. In future work, these effects may be explicitly taken into account to quantify uncertainties in the damage of these materials due to particle sizes and particle size distributions.

References

1. S. F. Hassan and M. Gupta, *Mater. Sci. Technol.* 20, 1383 **(2004)**.
2. S. Hwang, C. Nishimura, and P. G. McCormick, *Scripta Mater.* 44, 2457 **(2001)**.
3. L. Lu, M. Lai, and W. Liang, *Compos. Sci. Technol.* 64, 2009 **(2004)**.
4. I. Shao, P. M. Vereecken, C. L. Chien, P. C. Searson, and R. C. Cammarata, *J. Mater. Res.* 17, 1412 **(2002)**.
5. S. C. Tjong, *Adv. Eng. Mater.* 9, 639 **(2007)**.
6. N. Ramakrishnan, *Acta Mater.* 44, 69 **(1996)**.
7. S. Torquato, *Appl. Mech. Rev.* 44 **(1991)**.
8. S. Torquato, *Journal of the Mechanics and Physics of Solids* 45, 1421 **(1997)**.
9. S. Torquato, *Journal of the Mechanics and Physics of Solids* 46, 1411 **(1998)**.
10. S. Torquato, Random Heterogeneous Materials: Microstructure and Macroscopic Properties, Springer-Verlag, New York **(2002)**.
11. S. Torquato and S. Hyun, *J. Appl. Phys.* 89, 1725 **(2001)**.
12. Z. Hashin and S. Shtrikman, *Journal of the Mechanics and Physics of Solids* 10, 335 **(1962)**.
13. Z. Hashin and S. Shtrikman, *Journal of the Mechanics and Physics of Solids* 11, 127 **(1963)**.
14. J. Boussinesq, *Paris: Gauthier-Villars* 45, 108 **(1885)**.
15. Z. Hashin, *ASME Journal of Applied Mechanics* 50, 481 **(1983)**.
16. Z. Zhang and D. L. Chen, *Scripta Mater.* 54, 1321 **(2006)**.

Received: 15 May 2008. Accepted: 15 October 2008.